The role of subduction recycling on the selenium isotope signature of the mantle: Constraints from Mariana arc lavas

Timon Kurzawa[1*], Stephan König[1], Jeffrey C. Alt[2], Aierken Yierpan[1] and Ronny Schoenberg[1]

[1]Isotope Geochemistry, Department of Geosciences, Eberhard Karls University of Tübingen, Wilhelmstraße 56, 72074 Tübingen, Germany

[2]Department of Earth and Planetary Sciences, The University of Michigan, 1100 North University Avenue, Ann Arbor, MI 48109-1005, USA

*Corresponding author (phone: +49 7071 29-74991; e-mail: timon.kurzawa@uni-tuebingen.de)

Abstract

Investigating the isotope systematics and behavior of selenium in subduction zones provides valuable insights into mechanisms that contribute to chalcophile and moderately volatile element distribution between terrestrial reservoirs. In this study, we present high-precision Se isotope and Se-Te elemental data on subduction zone lavas from the Mariana arc system. Our results indicate that Se-Te concentrations are unaffected by degassing but are affected by sulfide segregation. In contrast, Se isotopes of submarine lavas are unaffected by both degassing and sulfide segregation and thus may preserve their magmatic source signature. Compared to the Se isotope composition of the current mantle estimate ($\delta^{82/76}$Se = 0.23±0.12‰, 2 s.d., n=5) that is based on mafic mantle-derived samples from diverse geodynamical settings but without any subduction-related origin, Mariana lavas show a larger overall range ($\delta^{82/76}$Se from 0.03 to −0.33‰, n=21) with a clear tendency towards lighter Se isotope compositions. The variable Se isotope signatures within the Mariana suite can further be attributed to different slab-derived fluid and melt-like subduction components. This provides evidence for a significant role of subduction recycling of altered oceanic crust, hydrothermal sulfides and pelagic sediments with possible implications for the Se isotope evolution of the crust-mantle system throughout geological time.

with possible implications for the Se isotope evolution of the crust-mantle system throughout geological time.

Keywords: Mariana arc; selenium isotopes; selenium; tellurium; subduction zone; chalcophile element recycling

1 Introduction

Constraining the behavior of elements in subduction zones provides valuable insights into their distribution and (re)cycling between surface and igneous reservoirs throughout Earth's evolution. The distribution of the chalcophile and moderately volatile elements sulfur (S), selenium (Se) and tellurium (Te) are of particular interest because they provide insights into Earth's volatile origin and evolution (König et al., 2014; Wang and Becker, 2013). Selenium and Te are ultra-trace elements with two orders of magnitude lower abundances in Earth's mantle compared to CI chondrites. Their abundances however, are still higher than expected from metal-silicate partitioning experiments (Rose-Weston et al., 2009), which predict S, Se and Te to be very effectively scavenged from Earth's mantle into its core during metal core formation. This may be reconciled with a late accretion of chondritic material (late veneer hypothesis; e.g. Kimura et al., 1974) following core-mantle differentiation. The relative abundances of S-Se-Te in mantle rocks believed to represent the primitive upper mantle (PUM) signature are near-chondritic, which was interpreted as evidence for replenishment of Earth's mantle by accretion of chondritic late veneer material (Wang and Becker, 2013). However, this interpretation conflicts with the non-chondritic sulfur isotopic composition of the Earth's mantle (Labidi et al., 2013), which has been attributed to partial incorporation of S into the Earth's core and thus substantial pre-Late Veneer existence of volatiles (Labidi et al., 2016). Alternatively, the observed near-chondritic Se/Te ratios in fertile peridotites might be the result of refertilization and thus represent secondary magmatic processes (Harvey et al., 2015; König et al., 2014; Lorand and Alard, 2010; Luguet et al., 2015). The fertile peridotite signature for adequate representation of a PUM model composition remains therefore controversially debated (König et al., 2015a; König et al., 2014; König et al., 2015b; Wang and Becker, 2013; Wang and Becker, 2015).

Investigation of the Se isotopic composition of the Earth's mantle offers a novel approach to investigate the origin and evolution of volatiles. This requires firm constraints on the Se isotopic composition of the different terrestrial reservoirs. Within this scope, the role of subduction zone processes on the Se isotope composition of the mantle is relevant because of large concentration and isotope differences between Earth's mantle and crust (Jenner, 2017; Jenner et al., 2012; Lissner et al., 2014; Rouxel et al., 2002; Yierpan et al., 2018). As in mid-ocean ridge settings, Se elemental signatures of subduction zone lavas are affected by sulfide segregation during magma differentiation (Brenan, 2015; Hamlyn et al., 1985; Jenner, 2017; Lissner et al., 2014) and these processes must therefore be considered in order to adequately interpret the Se isotope composition of arc lavas. Due to the different partitioning behavior of Se and Te in sulfides (i.e. partitioning into distinct sulfide phases), Se-Te systematics are a valuable tracer of the relative influence of the different sulfide populations involved during magmatic differentiation and partial melting (Brenan, 2015; Yierpan et al., 2019). Interpretation of the Se isotope composition of subduction zone lavas therefore benefits significantly from combined Se isotope and Se-Te elemental investigations. Recently, Kurzawa et al. (2017) and Yierpan et al. (2018) presented refined analytical techniques for both chemical purification and high-precision analyses of Se-Te concentrations and Se isotope compositions on samples with low total amounts of Se and Te. These analytical advancements provide the potential to investigate the Se isotope signature of low ng Se-bearing silicate rocks in the context of their Se-Te elemental signatures. This helps to evaluate the different petrogenetic processes involved in mantle melt evolution and ultimately to decipher the role of subduction recycling on the Se isotope composition of the mantle.

Studies on V, Fe and Tl isotopes (Prytulak et al., 2013; Prytulak et al., 2017; Williams et al., 2018) have been conducted on samples from the Mariana arc system to (i) investigate the oxygen fugacity of the mantle source (using V isotopes), to (ii) explore the interplay of sulfide saturation and segregation as well as crystal fractionation on the isotope composition of arc lavas (Fe and V isotopes) and to (iii) trace subduction zone inputs (using Tl isotopes). These studies concluded that Fe and V isotope signatures of magmatic rocks cannot directly be used as redox proxies without considering the influence of magmatic processes such as partial melting and differentiation. Yet, the timing of sulfide saturation and magnetite crystallization and associated isotope fractionations could be constrained.

In this study we focus on a suite of well-characterized, submarine arc lavas dredged from the Mariana subduction system (Fig. 1), which already have been the focus of a pioneering work on S isotopes (Alt et al., 1993). This suite may hence provide the geochemical background for first Se isotope constraints on chalcophile element recycling in subduction zones.

2 Geodynamic and geochemical context of sample materials

The Mariana arc-basin magmatic system (herein referred to as the Mariana system) extends over a distance of 2800 km (N-S) and constitutes the southern extension of the Izu-Bonin-Mariana subduction zone. The Mariana system is the result of westward subduction of the Pacific Plate along the Mariana trench beneath the Philippine Sea Plate initiated in the early Eocene (e.g. Stern and Bloomer, 1992; Stern et al., 2003). It can be subdivided into the Mariana island arc, which is an arcuate alignment of ~40 subaerial and submarine volcanoes, and the Mariana trough, an actively spreading back-arc basin (e.g. Pearce et al., 2005).

A total of 21 glassy samples from the submarine Mariana arc and trough sections (Fig. 1) were analyzed in this study. Among these are 12 samples from the active Mariana arc. These samples were either dredged (Fukujin, Eifuku and S. Daikoku) or collected by submersible (Kasuga) at collection depths of ~800-2900 mbsl (Alt et al., 1993). Additionally, 9 samples from two trough localities (18°N and 22°N) were analyzed, that were obtained by submersible or dredging at collection depths of ~2800-3700 mbsl. The samples are mainly basalts, basaltic andesites and andesites (Alt et al., 1993). Samples were petrographically classified into three groups: (i) 'glass', (ii) 'glassy' and (iii) 'microcrystalline' (see Alt et al., 1993). Some materials analyzed here have previously been analyzed including for S, Sr and Nd isotopes and major and trace element systematics (Alt et al., 1993 and references therein). These studies showed that back-arc lavas from 22°N and a single trough rock from 18°N (1846-9; Alt et al. (1993)) carry a strong arc signature, as inferred from trace element and Sr-Nd-Pb isotope systematics, which can be explained by addition of an arc component to a MORB mantle (e.g. Stern et al., 1990). Based on this observation, we suggest the subdivision of the following groups among the samples analyzed: back-arc samples at 18°N, arc-like samples at 22°N (and sample 1846-9 from 18°N) (where the back-arc basin intersects the arc) and arc samples from submarine volcanoes

(Kasuga, Fukujin, Eifuku, S.Daikoku). These subdivisions also account for different subduction components that comprise shallow, deep and total slab-derived contributions as expressed by Ba/Th, Th/Yb and Ba/Yb, respectively (Pearce et al., 2005). The shallow subduction contribution results from early dehydration of the slab and migration of fluids from the slab-mantle interface into the sub-arc mantle wedge (arc and back-arc). Deep subduction additions are explained as sediment-derived melt-like components (mainly arc). The flux of subduction components in not limited to vertical transport but also includes lateral transport (Stolper and Newman, 1994 and references therein). In previous studies, the sub-arc mantle wedge has been interpreted to act as chromatographic column diluting the subduction input in arc-distal areas. However, assessing these mechanisms in these arc-distal areas is not the aim of this study and we rather focus on how the different and variable subduction components influence the Se isotope systematics of arc-related melts.

3 Analytical techniques

3.1 Reagents, materials, major- and trace element analyses

Glass free of coatings and alteration was carefully handpicked from each sample, followed by multiple washing steps in dilute HCl and distilled water and were finally ground to powder (Alt et al., 1993). Sulfur concentrations of these samples were already published by Alt et al. (1993). In addition to Se isotope measurements and Se-Te concentration analyses, selected samples were also analyzed for major and trace element concentrations. All analyses were performed in the ISO-5 (US FED standards class 100) clean-room facilities of the Isotope Geochemistry at the University of Tübingen, Germany. All reagents used during digestion, sample preparation and measurements were distilled from MERCK Millipore Emsure™ grade HCl (37%) and HNO_3 (65%) using Savillex™ DST-1000 Acid Purification Systems. Reagents were diluted to required molarities to ±0.03 mol L^{-1} as checked by titration. Ion exchange resins, beakers, pipette tips and centrifuge vials were pre-cleaned with multi-step HCl and HNO_3 treatments. A Merck Millipore Milli-Q™ system was employed to further purify de-ionized water to 18.2 MΩ·cm at 25 °C.

Previously determined major element data was complemented and trace elements were measured for the entire Mariana sample suite (Alt et al., 1993) during this study using a ThermoFisher Scientific iCAP Qc quadrupole ICP-MS housed at the Isotope Geochemistry Laboratory at the University of Tübingen following the analytical procedure by Albut et al. (2018). Due to limited sample material, all major and trace element concentrations of samples were determined together with rock reference materials AGV-2 (for major element data, n=2) and BHVO-2 and BIR-1a (for trace element data, n=2 and 1, respectively). Analytical precision for most analyzed trace elements is better than 2% r.s.d. except for Be, As, W and U with analytical precisions better than 5% r.s.d. Obtained trace element concentrations of rock reference materials match those reported by Jochum et al. (2016) (see Supplemental Information). For major element analysis, 0.1 g of homogenized sample material was fused together with 0.5 g of Spectromelt® to produce a fused glass bead, which was subsequently dissolved in 0.45 mol L^{-1} HNO_3 in a Teflon beaker agitated in an ultrasonic bath and diluted by addition of an internal standard solution before final measurement. For determination of trace element concentrations, 0.02 g homogenized powder of each sample were weighted into Teflon beakers and digested at 120°C in a mixture of concentrated HF and HNO_3 (5:1, v/v). After dry down, the samples were taken up in 6 mol L^{-1} HCl and heated in closed beakers to break up existing fluoride complexes. The sample solutions were again evaporated to dryness, converted to nitrite form and subsequently diluted with an internal standard solution before final measurement.

3.2 Se concentration analyses

Pre-determination of Se concentration of an unknown sample is required in order to know the amount of double spike to be added to the sample for precise Se isotope analysis with ideal double spike-sample ratio of ~1:1 (Kurzawa et al., 2017). For the pre-determination of Se concentrations via isotope dilution, we followed the procedure described by Yierpan et al. (2018). For this, we weighed 0.02 g sample material (equivalent to 2 ng total Se assuming a Se concentration of 100 ng g^{-1}) in Teflon beakers, added an adequate amount of ^{74}Se-^{77}Se double spike and digested the mix with an acid mixture of 5:1 (v/v) conc. HF : conc. HNO_3 in closed Teflon beakers at 85°C. The digested samples were then dried at 65°C followed by conversion, heating and dry down steps (see Yierpan et al., 2018)

in 6 mol L^{-1} HCl before Fe was removed by means of anion exchange chromatography. Fe-free cuts were then diluted to 0.5-1 ng mL^{-1} Se and finally measured on the iCAP Qc ICP-MS using hydride generation following the protocol of Yierpan et al. (2018).

3.3 Se isotope and Te concentration analyses

Chemical purification of Se and Te for subsequent Se isotope and Se-Te concentration analyses was achieved following the protocol by Yierpan et al. (2018) as it allows to simultaneously purify Se and Te from a single sample digest with high yields. Briefly, this involves weighing sample material equivalent to ~30 ng Se (exact Te amount uncritical) into conventional perfluoralkoxy (PFA) beakers, adding adequate amounts of ^{74}Se-^{77}Se double spike (1:1; sample Se : double spike Se) and ^{125}Te single spike (exact single spike amount less critical) and digesting the sample-spike mixtures in an acid mixture of 5:1 (v/v) conc. HF : conc. HNO_3 in closed beakers on a hotplate at 85°C for 48 hours. Se and Te were purified from sample solutions by a two-step ion exchange chromatography. In a first step, we employed an anion exchange column to remove Fe and collect purified Te. In a second step, Se was purified using a cation exchange column to remove remaining cations. Te concentrations were then determined by hydride generator quadrupole ICP-MS on the iCAP Qc instrument and Se isotopes and concentrations were measured by hydride generation multi-collector ICP-MS on the ThermoFisher Scientific Neptune*Plus*™ instrument of the Isotope Geochemistry laboratory, University of Tübingen. Typical signals on ^{82}Se (using an amplifier resistor of 10^{11} Ω) on a 30 ng mL^{-1} Se solution with operating parameters similar to those reported by Kurzawa et al. (2017) generally are 0.8-0.9 V. During Te concentration measurements on the iCAP Qc ICP-MS using similar operating parameters to those of Yierpan et al. (2018), ~55000cps on ^{126}Te were obtained for a Te standard solution of 0.5 ng mL^{-1}. Se isotopes and Te concentrations of samples were determined at similar signal intensities compared to those of standard solutions. For detailed descriptions of analytical techniques employed see Kurzawa et al. (2017) and Yierpan et al. (2018). All Se isotope compositions obtained during this study are reported relative to the NIST-3149 Se reference solution. Measurements of the inter-laboratory standard solution MH-495 yielded an average value of $\delta^{82/76}Se$ of −3.25±0.08‰ (2s.d., n=26, 30 ng mL^{-1} solutions, see Supplemental Information), in agreement with previous studies

(Kurzawa et al., 2017; Yierpan et al., 2018 and references therein). The external reproducibility for sample materials was derived from two multiple digested samples (arc-like 1881-4; Kasuga 1880-3 (K2)) during different measurement sessions and is 0.10‰ (2 s.d., n=3 and n=6, respectively; Supplemental Information). All samples were measured together with the international rock reference material USGS BHVO-2 that has been published by Yierpan et al. (2018). Further, we provide Se isotope and Se-Te concentration data for the international rock reference materials JB-2 and JB-3 (Geological Survey of Japan). Obtained Se-Te concentrations are in agreement with data reported in the literature (see Supplemental Information). Long-term analytical reproducibility for both Se and Te concentration determinations are ~3% r.s.d. The main advantage of the procedure by Yierpan et al. (2018) followed here is that it yields very low blanks. Accurate isotopic compositions of procedural blanks cannot be determined because blank levels are always insignificant (at background level; e.g., ~0.05 and 0.01 ng for Se and Te, respectively; see Yierpan et al. (2019)). However, Kurzawa et al. (2017) showed high accuracy for low Se-containing solutions with various blank levels (up to 1 ng) that confirms a negligible blank contribution for a given isotopic composition.

4 Results

4.1 Major and trace elements

All samples show 48 to 61 wt.% SiO_2 and 2 to 9 wt.% MgO (Tab. 1) and are classified as basalts, basaltic andesites, andesites. Relative to the back-arc samples (MgO between 5 to 9 wt.%) and with the exception of the Kasuga samples, the arc samples are more differentiated showing MgO contents of 2 to 4 wt.%. The Kasuga samples are more primitive as indicated by lower SiO_2 and higher MgO contents of <55 wt.% and >5 wt.%, respectively. The samples from S.Daikoku, Eifuku, Fukujin and both back-arc localities follow the tholeiitic fractionation trend whereas samples from Kasuga follow calc-alkaline to shoshonitic fractionation trends (Alt et al., 1993). In terms of major element composition samples from both back-arc localities (18°N and 22°N) are indistinguishable from each -other. Our new trace element data are in accordance with previous observations (Stern et al., 2003 and references therein) in that primitive mantle normalized trace element diagrams (after Palme and

O'Neill, 2014) for the Mariana arc and trough samples all show marked enrichments in large ion lithophile elements and light rare earth elements such as Rb, Ba, U, K, Pb ,Sr, La and Ce, show arc-typical relative depletions in high field strength elements (HFSE) (e.g. Nb, Ta, Zr, Hf) and relatively low heavy rare earth element concentrations (e.g. Tb, Er, Yb) (Fig. A.1). They share these characteristics with other arc volcanic rocks from the Mariana arc (e.g. Elliott et al., 1997). In addition, our new trace element data are in agreement with the previous observation (section 2.1 and Pearce et al., 2005) that the back-arc samples are dominated by slab-derived fluid enrichment (elevated Ba/Th compared to primitive mantle) and the arc samples additionally contain a marked sediment-melt subduction component (similar Ba/Th but higher Th/Yb and Ba/Yb than the back-arc suite).

4.2 S-Se-Te concentrations

The arc samples exhibit S contents in the range of 10 to 200 µg/g. Compared to those, back-arc and arc-like samples are characterized by higher S contents between 200-930 µg/g (Alt et al., 1993). Selenium concentrations of back-arc samples are on average 153±55 ng g^{-1} (1 s.d., n=4), similar to those from arc-like samples with an average of 138±42 ng g^{-1} (1 s.d., n=5) (Fig. 4a). In contrast, the arc samples show lower Se contents with an average of 111±32 ng g^{-1} (1 s.d., n=12) (Table 1) and can vary significantly between volcanoes and even within one individual volcano (e.g. Kasuga). Sulfur/Selenium ratios of back-arc and arc-like samples range from 2190 to 8230 and 1450 to 5110, respectively (Fig. 3d). The arc samples show generally lower S/Se ratios in the range of 120 to 1680 (Fig. 3d).

Tellurium concentrations of back-arc and arc-like samples show average concentrations of 4.0±2.3 ng g^{-1} (1 s.d., n=4) and 2.4±1.5 ng g^{-1} (1 s.d., n=5), respectively (Fig. 4b). The arc samples are characterized by Te concentrations with an average of 2.1±2.0 ng g^{-1} (1 s.d., n=12). The Te concentrations of some arc samples (n=5, e.g. back-arc sample 1846-9) analyzed by Yi et al. (2000) are in good agreement with those obtained in this study. The Se-Te ratios are controlled by variable Te concentrations and are most variable within the arc samples ranging from 14 to 481. It is noteworthy, that the Se/Te ratios of the Kasuga volcano are among the lowest of all arc samples with typical Se/Te

between 14 and 31. Two samples from Fukujin are characterized by very low Te concentrations (<1 ng g^{-1}; see Table 1) and thus have the highest Se/Te ratios (393 and 481, respectively).

4.3 Se isotope composition

The average $\delta^{82/76}$Se of the back-arc samples is −0.03±0.03‰ (2 s.d., n=4) whereas the average $\delta^{82/76}$Se of the arc-like samples is −0.21±0.16‰ (2 s.d., n=5) (Fig. 2 and 5a). The arc samples exhibit Se isotopic compositions that average at −0.13±0.17‰ (2 s.d., n=12) (Fig. 2 and 5a). The Se isotope compositions of the samples are not related to silicate differentiation as inferred from the absence of covariation of MgO and $\delta^{82/76}$Se (Fig. 5a). Furthermore, the $\delta^{82/76}$Se of the samples are unrelated to the collection depths (Fig. 3b).

Interestingly, the back-arc samples are isotopically heavier than the arc and arc-like samples, which overlap in their Se isotope composition with recent Se isotope data of MORBs from the Pacific Antarctic Ridge (PAR; Yierpan et al., 2019). However, it is very important to note that, Mariana samples originate from a different mantle domain than Pacific-type MORBs. Volpe et al. (1990) concluded from Sr, Nd and Pb isotope ratios of Mariana Trough basalts (equivalent to back-arc samples analyzed in this study), that the mantle beneath the back-arc region of the Mariana arc is isotopically similar to average Indian-type MORB. Most likely, this also applies to the mantle wedge beneath the Mariana arc, similar to complex dynamics revealed for other SW Pacific arcs (e.g. König et al., 2007; Schuth et al., 2011). In contrast, PAR basalts originate from the Pacific mantle domain that is isotopically depleted compared to the Indian mantle domain (Ito et al., 1987). Thus, the Indian mantle domain resembles an enriched mantle reservoir compared to the Pacific mantle domain, which precludes a direct comparison of the PAR data and our Mariana data. Given the absence of literature $\delta^{82/76}$Se data for the Indian mantle domain, the Mariana pre-subduction wedge may be best represented by melts that originate from enriched reservoirs that are isotopically heavier as indicated also by the heavier back-arc compared to arc lavas analyzed here (Fig. 2). Hence, a suitable Mariana pre-subduction background is provided by the most recent data of worldwide, non-subduction-related basalts (BHVO-2, BCR-2, BIR-1a and BE-N) by Yierpan et al. (2018) and the reported peridotite (PCC-1) value of Rouxel et al. (2002), which yield an average $\delta^{82/76}$Se of 0.23±0.12‰ (2 s.d., n=5).

Compared to this value, all Mariana samples, including for the back-arc, show isotopically lighter Se isotope compositions (Fig. 2). Note, that especially the arc and arc-like samples display a greater variability in their $\delta^{82/76}$Se (e.g. Fig. 2) compared to the more homogeneous and slightly isotopically heavier back-arc lavas. We conducted *t*-tests to evaluate the statistical significance of the different averages of the distinct sample suites relative to the pre-subduction mantle. The three obtained two-tailed P values for the back-arc, the arc-like and the arc samples each relative to the pre-subduction mantle equal $t(7)=4.18$, $p=0.0042$, $t(8)=4.92$, $p=0.0012$ and $t(15)=4.27$, $p=0.0007$, which are all statistically very significant.

5 Discussion

5.1 No effect of degassing on Se isotope signatures of submarine Mariana lavas

Previous work on Mariana arc lavas showed heavier S isotope signatures compared to the mantle, which was suggested to mirror recycling of subducted sediments (Alt et al., 1993). A trend of decreasing S contents (Fig. 3a) and low S concentrations in highly vesicular Mariana lavas suggests that partial extrusive degassing of S can occur in submarine environments despite the great pressures of overlying water columns (Alt et al., 1993; Davis et al., 1991). Considerable differences in S concentrations of lavas erupted under submarine conditions may result from partial eruptive degassing, the degree of crystal fractionation, different conditions and percentages of partial melting and variations in source conditions (Davis et al., 1991). An assessment of these processes and their role on S isotope compositions is beyond the scope of this study. Importantly, Se contents and Se isotope compositions of our samples do not systematically change with water depths (Fig. 3b, c), nor do Se contents correlate with Se isotope compositions (Fig. 5b). Moreover, Se concentrations of our samples are independent from S as inferred from a lack of covariation between these elements (Fig. 3d) in contrast to a correlation of S/Se ratios controlled by S (not shown). Therefore, irrespective of the process affecting S, we rule out Se loss and Se isotope fractionation due to eruption-related degassing.

Recently, Jenner et al. (2010) reported similar Se concentrations in volcanic rocks derived from the Manus back-arc basin (north-east of Papua New Guinea) compared to MORB and concluded, that the Se contents remain unchanged during eruption associated degassing, which is in accordance with our conclusion. The decoupling of Se from S in terms of their degassing potential might be due to the fact that Se becomes oxidized only at elevated fO_2, or Eh, compared to S as earlier proposed by Jenner et al. (2010 and references therein). This implies that Se is retained whereas S (oxidized at given Eh) is lost.

5.2 Magmatic differentiation

Although submarine Mariana arc lavas from the shallowest depths contain the lowest S contents (Table 1), back-arc lavas from rather constant and great depths (>3000 mbsl) also show very variable S contents (~200-1000 µg/g). This suggests that a process unrelated to changing water column pressure (such as potential degassing and magmatic differentiation) also affected the S contents of the lavas. Since all our samples show MgO contents between ~9 and 2 wt.% (Tab. 1) the effect of magmatic differentiation and potential sulfide segregation needs to be considered when interpreting chalcophile element concentrations and in particular potential Se isotope variations.

Geochemical evidence for sulfide segregation stems from trends of chalcophile element concentrations (Cu, Se and Te) and V/Sc versus MgO (Fig. 4) (Jenner, 2017 and references therein). Before ~7 wt.% MgO the concentrations of Se, Te (and some Cu) increase, followed by a drop in concentrations (Fig. 4a-c). A different phase than sulfide has to account for the observed changes in Se-Te-Cu concentrations, because the melt is under-saturated in sulfides at this stage of melt differentiation (Jenner et al., 2015; Jenner et al., 2010). In the case of the platinum group elements (PGEs), a Pt-rich alloy has been identified to be the most likely source of PGE depletion during early stages of fractional crystallization before the magnetite crisis and segregation of sulfides (Jenner et al., 2015; Park et al., 2013). Thus, it is likely that Se and (especially) Te are concentrated in alloys (e.g. tellurides; König et al., 2015a) that crystallize from sulfide under-saturated melts.

From ~6 to ~3 wt.% MgO, Se and Cu concentrations increase whereas Te concentrations still decrease, which might be due to incorporation of Te into Pt-Te-alloys (Fig. 4b). Note, that the

observed trend seen for Cu concentrations (Fig. 4c) is also evident from Cu data reported in the literature (Jenner et al., 2015; Williams et al., 2018). At ~3 wt.% MgO and contents of Cu, Se and Te in the melt show a pronounced scatter, possibly related to appearance of sulfides, which are not fully segregating (previously inferred by Williams et al. (2018)).

At 2.8 wt.% MgO, magnetite appears on the liquidus as inferred from the onset of decreasing V/Sc that is accompanied with a decrease in the $Fe^{3+}/\sum Fe$ ratio leading to a decline in fO_2 (Jenner et al., 2010). At this stage sulfide becomes saturated in the melt and finally segregates, thus scavenging Se, Te and Cu, albeit to different extents (more pronounced decrease of Cu and Te contents compared to Se; Fig. 4). This is related to a lower sulfide-silicate melt partition coefficient of Se compared to Cu.

Whereas the exact processes responsible for the unsystemtic variations in Cu, Se and Te concentrations remain to be constrained, it is important to investigate potential correlations between Se concentrations and an index of differentiation, such as MgO, with Se isotope variations. Previous studies (Prytulak et al., 2017; Williams et al., 2018) involving Mariana arc lavas showed that for both V and Fe, significant isotope fractionation is induced as a consequence of magnetite fractionation and sulfide segregation, respectively. Both studies identified heavier isotope compositions following the 'magnetite-crisis' at ~2.8 wt.% MgO, consistent with preferential scavenging of isotopically light V and Fe into magnetite and sulfide phases.

Such a link between sulfide saturation and Se isotope fractionation is not observed in our study. No trend between the Se isotope composition and MgO or Se is seen (Fig. 5a,b), which suggests that magmatic differentiation processes significantly affect both Se and other chalcophile element contents of the samples analyzed (Fig. 4), but do not result in Se isotope fractionation. This is in agreement with observations and conclusions based on a dry magmatic suite from the PAR (Yierpan et al., 2019). As neither degassing nor magmatic differentiation affect the Se isotope compositions of our samples, the isotopic variations among Mariana samples, particularly systematic differences between back-arc and arc samples are most likely related to their respective source composition.

5.3 Different subduction components and their influence on the Se isotope composition of arc lavas

The $\delta^{82/76}$Se signatures of Mariana lavas show a relatively large range and overall lower values compared to a rather confined range for the Mariana pre-subduction mantle, represented by basaltic melts and peridotite from intraplate and ridge settings, but without any subduction-related origin. Thus, $\delta^{82/76}$Se signatures of Mariana lavas seem indeed intrinsic to their subduction zone origin (Fig. 2). The Se isotope compositions of the Mariana lavas represent that of their mantle sources in contrast to their elemental budget that is compromised by magmatic differentiation (see section 5.2). Se isotopes of Mariana lavas may thus trace the slab-derived contribution and be related to potential recycling of Se in subduction zones. Although the Mariana system is highly complex, the natures of subduction components (i.e. fluid-like and melt-like components, see sections 2 and 4.1) added to the sub-arc mantle are broadly classified via different incompatible trace element systematics (Pearce et al., 2005). Any covariations between these proxies of subduction components and Se isotope compositions could therefore help to assess potential subduction recycling of Se. Slab-derived fluids and sediment melts may influence the Se isotope compositions of Mariana lavas to different extents. Figure 6a shows variable Ba/Th and Th/Yb ratios indicating that Mariana arc lavas are affected by both subduction components as has been documented in the literature (e.g. Elliott et al., 1997). Figure 6b shows the Se isotope compositions of all Mariana samples relative to Ba/Th, indicating slab-derived fluid enrichments (termed shallow subduction component by Pearce et al. (2005)). It can be observed that Mariana lavas all show lower $\delta^{82/76}$Se at somewhat higher Ba/Th compared to the Mariana pre-subduction mantle albeit some scatter exists in the dataset (Fig. 6b). Slab-derived sediment melts were termed deep subduction component by Pearce et al. (2005) and are indicated for instance by elevated Th/Yb in arc samples. Interestingly, these arc samples also extend to slightly heavier Se isotope compositions relative to slab-fluid dominated back-arc and arc-like samples (Fig. 6c). The influence of a sediment melt on the arc samples is also expressed by high La/Sm ratios (Elliott, 2003), which indeed show a positive trend with $\delta^{82/76}$Se but no trend with indicators for magmatic differentiation such as MgO contents (Fig. A.2).

Although back-arc and arc-like samples mostly overlap in their relatively low Th/Yb, they can be distinguished based on their respective $\delta^{82/76}$Se (Fig. 6c). In particular the back-arc samples with their highest relative $\delta^{82/76}$Se do not match the tendencies observed for the other sample suites, which could be attributed to their rather distinct origin within the subduction zone. Indeed, the location of the back-arc samples lies ~350 km away from that of the arc-like samples (Fig. 1). In contrast, arc and arc-like samples originate from relatively restricted areas, respectively. These two groups however share the same subtle tendency between $\delta^{82/76}$Se and Th/Yb (Fig. 6c), which is in agreement with a strong arc signature previously found in back-arc lavas from 22°N (see section 2; Stern et al. (1990)). The back-arc samples fall off this trend, possibly reflecting a different source due to the remote setting. It seems clear however, that all samples experienced slab fluid addition revealed by increased Ba/Th and offset to lower $\delta^{82/76}$Se compared to the pre-subduction mantle. Again, the distinction between shallow and deep subduction contribution based on Ba-Th-Yb systematics and the observation that sediment melts are more dominant in the arc samples compared to the back-arc samples is entirely based on a previous classification (Pearce et al., 2005). Reasons for a similar shallow and less pronounced deep subduction signature in back-arc lavas may be a chromatographic effect and dilution by back-arc melts (Stolper and Newman, 1994). Overall, it seems that shallow slab fluids can explain lower $\delta^{82/76}$Se, whereas deep-derived sediment melts may carry a heavier Se isotope signature that raises the $\delta^{82/76}$Se again (i.e. buffer the initial slab-fluid signature). Hence, slab-derived fluids and sediment melts (Fig. 6a, Ba/Th vs. Th/Yb) may shift $\delta^{82/76}$Se in arc lavas to opposing directions, where the relative proportion of these subduction components ultimately determines the direction of tendencies among suites. As a result, the total subduction addition, expressed by Ba/Yb (Fig. 6d), may be the best approximation of a net recycling signature (Pearce et al., 2005) that seems to produce lower overall $\delta^{82/76}$Se compared to the Mariana pre-subduction mantle. Further studies that examine in more detail the effects of different types of subduction components are clearly required. Moreover, it remains to be investigated if and how a net contribution of subduction components to arc lavas relate to the Se isotope signature of the subduction input. In the case of S, the heavier δ^{34}S of Mariana lavas compared to the mantle has been linked to recycling of subducted sediments (Alt et al., 1993). Sediments in addition to altered oceanic crust containing hydrothermal sulfides indeed show variable Se isotope

compositions (e.g. Mitchell et al., 2016; Rouxel et al., 2004; Rouxel et al., 2002). Therefore, it is necessary to assess if recycling of these materials might in principle account for the Se isotope compositions observed in subduction zone magmas.

5.4 Recycling of subducted surface material as possible source for Se isotope variability in Mariana arc lavas

Marine sediments have been the focus of numerous Se isotope studies (e.g. Mitchell et al., 2016 and references therein). So far, available data from the literature comprises shales of various ages (Archean to present day) and depositional environments (open marine and marine basins) with distinct conditions (euxinic, anoxic, suboxic and oxic) (Mitchell et al., 2016). Stüeken et al. (2015) identified a statistically significant shift in the Se isotope composition from predominantly positive (0.63±0.67‰; 2 s.d., n=169) to negative (−0.28±0.88‰; 2 s.d., n=240) $\delta^{82/76}$Se values from Precambrian to Phanerozoic samples (Fig. 2; see also Fig. 3a in Stüeken et al., 2015). Taken together, the Se isotope compositions of all these samples combined with other published $\delta^{82/76}$Se data (e.g. Mitchell et al., 2016) are in the range of −3 to +3‰ (Fig. 2; see also Mitchell et al., 2016). This suggests that not the entire Se isotope variation of all hitherto analyzed sediments qualify as endmembers to constrain potential sediment recycling in a modern subduction zone system. Instead, a narrower isotopic range of only modern sediments can be considered to begin with. In addition to age, the depositional setting may also be critical. Isotope fractionations in low-temperature environments can be large as inferred from laboratory experiments (Johnson and Bullen, 2004) and the wide range of reported $\delta^{82/76}$Se of sediments (e.g. Mitchell et al., 2016; Rouxel et al., 2002; Stüeken et al., 2015). Even these modern surface Se isotope variations exceed that identified in Mariana lavas by far but all show average $\delta^{82/76}$Se that are distinctly negative (Fig. 2). Thus, subduction recycling of surface material may indeed account for the isotopic offset of Mariana lavas compared to the Mariana pre-subduction mantle range.

Deep-sea sediments of the uppermost stratigraphic section from Site 1149 ODP 129, which are subducted beneath the Izu-Bonin-Arc as part of the Izu-Bonin-Mariana subduction system, have been analyzed for Se isotopes (Rouxel et al., 2002). These sediments have an average Se isotope composition of −0.42±1.44‰ (2 s.d., n=3, Rouxel et al., 2002), in agreement with input of, on

average, isotopically light Se during subduction. However, in addition to pelagic sediments, subducted volcaniclastic turbidites have been identified as another major source of melt-like subduction components affecting the geochemistry of arc lavas in the northern part of the Mariana arc (Tollstrup and Gill, 2005). Moreover, isotopically light, hydrothermally altered basalt may also contribute to an isotopically light subduction input (−1.33±0.31‰, 2 s.d., n=2; Rouxel et al., 2002). Overall, although the proportion of altered versus unaltered oceanic crust to a net subduction input is difficult to constrain, the role of subducted sulfides need to be considered.

Due to its chalcophile behavior Se is predominantly hosted by sulfides both in the mantle and slab (e.g. Guo et al., 1999; Hattori et al., 2002; König et al., 2015a; König et al., 2014). Thus, hydrothermal sulfides may constitute important subduction input material and published data show an average Se isotope composition of −1.36±2.82‰ (2 s.d., n=77; Rouxel et al., 2004; Rouxel et al., 2002) with the most extreme values up to −4.75‰. This is in agreement with recent analyses of hydrothermal pyrite minerals, albeit from a continental setting, showing a record of $\delta^{82/76}$Se ranging from −4.48±0.09‰ to −0.39±0.09‰ (2 s.d., n=10) with an average of −2.73±0.09‰, altogether confirming the pronounced, isotopically light hydrothermal sulfide signatures for Se (König et al., 2019). Hydrothermal sulfides together with pelagic clays may be among the first phases to destabilize during subduction and therefore significantly contribute to slab-derived fluid signatures. The importance of sulfides in the recycling of chalcophile elements is supported by the observation of migrating S-bearing fluids up the subduction interface after liberation of sulfide from sediments and altered basalt at shallower depth (Mottl et al., 2004). It has further been suggested that S is released from magmatic sulfides in sediments and the oceanic crust itself by extensive recrystallization during high-pressure metamorphism (Li et al., 2016), possibly amplifying Se recycling. However, some S enters deeper parts of the subduction zone as indicated by sulfide inclusions in garnets from eclogites that grew during prograde metamorphism (Li et al., 2016). This sulfur might be liberated by subduction components that contribute to enrichment of the deeper sub-arc mantle wedge. In summary, the complex combination of pelagic and volcaniclastic sediments, altered and unaltered oceanic crust and sulfides altogether could account for the relatively lighter Se isotope signatures of Mariana lavas compared to the pre-subduction mantle (Fig. 2).

A pronounced shift in the average Se isotope composition of marine sediments before and after ca. 550 Ma ($\Delta_{Precambrian-Phanerozoic} \approx 0.91‰$; Stüeken et al. (2015)) was recently reported. This shift was interpreted to be the result of increased oxidative weathering and more pronounced continental mobilization of Se following Earth's second atmospheric oxygen increase ca. 550 Ma ago (Neoproterozoic Oxygenation Event, NOE). Progressive subduction of this isotopically lighter average Se isotope input may have had an impact on the secular Se isotope composition of the Earth's upper mantle after ca. 550 Ma, possibly mirroring the NOE. Such a link between stepwise atmospheric oxygenation and mantle evolution has previously been invoked for redox-sensitive uranium isotope systematics (Andersen et al., 2015). Subduction recycling of Se may not only produce larger and systematic Se isotope variations in Mariana lavas compared to the Mariana pre-subduction mantle but also, make Se isotopes a tool to investigate links between Earth's interior and atmospheric oxygenation throughout geological history.

6 Conclusions

The first case study involving stable Se isotopes in arc and back-arc lavas provides significant new insights into the systematics of this chalcophile and moderately volatile element in subduction zones. The Se isotope signature of submarine Mariana lavas is not affected by degassing and, unlike the elemental Se budget, not affected by magmatic differentiation. Therefore, the $\delta^{82/76}$Se of submarine arc lavas may retain its source signature. This signature is likely enriched by melt-like and fluid-like subduction components derived from the subducting Pacific crust and overlying sedimentary cover. Mariana samples show a tendency to become isotopically lighter from the back-arc to arc(-like) lavas, possibly reflecting a decreasing chromatographic effect of the overlying mantle wedge and increasing influence of a fluid signature. Addition of a sediment melt-like subduction component seems to buffer this fluid-induced signature as observed in Mariana arc samples. Due to these complex contributions of subduction components, Se isotope compositions of Mariana lavas show a larger range and are overall lighter than the pre-subduction mantle range that comprises peridotite and non-subduction related worldwide mantle melts. Possible slab-derived contributions may be traced back to subduction recycling of isotopically light Se input such as modern sediments and altered sulfide-bearing oceanic

crust. Subduction recycling of Se may also have had an impact on the secular Se isotope composition of the Earth's upper mantle, because of a considerable shift to lighter average $\delta^{82/76}$Se in sediments that was attributed to the Neoproterozoic Oxygenation Event ca. 550 Ma ago. Further work on Se isotope systematics in arc lavas should therefore be dedicated to the different roles of variable subduction components and the possible links between atmospheric oxygenation, Se recycling and isotopic evolution of the mantle through geological time.

7 Acknowledgements

This work was funded by an ERC Starting Grant (O2RIGIN, 636808) to Stephan König. We acknowledge laboratory support by Ilka Kleinhanns and Elmar Reitter and help with major and trace element analyses by Bernd Steinhilber. This study benefited from constructive reviews by Frances Jenner, an anonymous reviewer and Catherine Chauvel, who also is thanked for editorial handling.

8 References

Albut, G., Babechuk, M.G., Kleinhanns, I.C., Benger, M., Beukes, N.J., Steinhilber, B., Smith, A.J., Kruger, S.J., Schoenberg, R., 2018. Modern rather than Mesoarchaean oxidative weathering responsible for the heavy stable Cr isotopic signatures of the 2.95 Ga old Ijzermijn iron formation (South Africa). Geochim. Cosmochim. Acta, 228: 157-189.

Alt, J.C., Shanks, W.C., Jackson, M.C., 1993. Cycling of sulfur in subduction zones: The geochemistry of sulfur in the Mariana Island Arc and back-arc trough. Earth Planet. Sci. Lett., 119(4): 477-494.

Andersen, M.B., Elliott, T., Freymuth, H., Sims, K.W., Niu, Y., Kelley, K.A., 2015. The terrestrial uranium isotope cycle. Nature, 517(7534): 356-359.

Brenan, J.M., 2015. Se–Te fractionation by sulfide–silicate melt partitioning: implications for the composition of mantle-derived magmas and their melting residues. Earth Planet. Sci. Lett., 422: 45-57.

Davis, A.S., Clague, D.A., Schulz, M.S., Hein, J.R., 1991. Low sulfur content in submarine lavas: An unreliable indicator of subaerial eruption. Geology, 19(7): 750-753.

Elliott, T., 2003. Tracers of the slab. Inside the subduction factory: 23-45.

Elliott, T., Plank, T., Zindler, A., White, W., Bourdon, B., 1997. Element transport from slab to volcanic front at the Mariana arc. Journal of Geophysical Research-Solid Earth, 102(B7): 14991-15019.

Gale, A., Dalton, C.A., Langmuir, C.H., Su, Y., Schilling, J.G., 2013. The mean composition of ocean ridge basalts. Geochem. Geophys. Geosyst., 14(3): 489-518.

Guo, J.F., Griffin, W.L., O'Reilly, S.Y., 1999. Geochemistry and origin of sulphide minerals in mantle xenoliths: Qilin, southeastern China. J. Petrol., 40(7): 1125-1149.

Hamlyn, P.R., Keays, R.R., Cameron, W.E., Crawford, A.J., Waldron, H.M., 1985. Precious Metals in Magnesian Low-Ti Lavas - Implications for Metallogenesis and Sulfur Saturation in Primary Magmas. Geochim. Cosmochim. Acta, 49(8): 1797-1811.

Harvey, J., König, S., Luguet, A., 2015. The effects of melt depletion and metasomatism on highly siderophile and strongly chalcophile elements: S–Se–Te–Re–PGE systematics of peridotite xenoliths from Kilbourne Hole, New Mexico. Geochim. Cosmochim. Acta, 166: 210-233.

Hattori, K.H., Arai, S., Clarke, D.B., 2002. Selenium, tellurium, arsenic and antimony contents of primary mantle sulfides. The Canadian Mineralogist, 40(2): 637-650.

Ito, E., White, W.M., Göpel, C., 1987. The O, Sr, Nd and Pb isotope geochemistry of MORB. Chem. Geol., 62(3): 157-176.

Jenner, F.E., 2017. Cumulate causes for the low contents of sulfide-loving elements in the continental crust. Nat. Geosci., 10(7): 524-529.

Jenner, F.E., Arculus, R.J., Mavrogenes, J.A., Dyriw, N.J., Nebel, O., Hauri, E.H., 2012. Chalcophile element systematics in volcanic glasses from the northwestern Lau Basin. Geochem. Geophys. Geosyst., 13(6).

Jenner, F.E., Hauri, E.H., Bullock, E.S., Konig, S., Arculus, R.J., Mavrogenes, J.A., Mikkelson, N., Goddard, C., 2015. The competing effects of sulfide saturation versus degassing on the behavior of the chalcophile elements during the differentiation of hydrous melts. Geochemistry Geophysics Geosystems, 16(5): 1490-1507.

Jenner, F.E., O'Neill, H.S.C., Arculus, R.J., Mavrogenes, J.A., 2010. The Magnetite Crisis in the Evolution of Arc-related Magmas and the Initial Concentration of Au, Ag and Cu. J. Petrol., 51(12): 2445-2464.

Jochum, K.P., Weis, U., Schwager, B., Stoll, B., Wilson, S.A., Haug, G.H., Andreae, M.O., Enzweiler, J., 2016. Reference Values Following ISO Guidelines for Frequently Requested Rock Reference Materials. Geostand. Geoanal. Res., 40(3): 333-350.

Johnson, T.M., Bullen, T.D., 2004. Mass-dependent fractionation of selenium and chromium isotopes in low-temperature environments. Rev. Mineral. Geochem., 55(1): 289-317.

Kimura, K., Lewis, R.S., Anders, E., 1974. Distribution of gold and rhenium between nickel-iron and silicate melts: implications for the abundance of siderophile elements on the Earth and Moon. Geochim. Cosmochim. Acta, 38(5): 683-701.

König, S., Eickmann, B., Zack, T., Yierpan, A., Wille, M., Taubald, H., Schoenberg, R., 2019. Redox induced sulfur-selenium isotope decoupling recorded in pyrite. Geochim. Cosmochim. Acta, 244: 24-39.

König, S., Lissner, M., Lorand, J.-P., Bragagni, A., Luguet, A., 2015a. Mineralogical control of selenium, tellurium and highly siderophile elements in the Earth's mantle: Evidence from mineral separates of ultra-depleted mantle residues. Chem. Geol., 396: 16-24.

König, S., Lorand, J.-P., Luguet, A., Pearson, D.G., 2014. A non-primitive origin of near-chondritic S–Se–Te ratios in mantle peridotites; implications for the Earth's late accretionary history. Earth Planet. Sci. Lett., 385: 110-121.

König, S., Luguet, A., Lorand, J.-P., Lissner, M., Graham Pearson, D., 2015b. Reply to the comment on "A non-primitive origin of near-chondritic S–Se–Te ratios in mantle peridotites: Implications for the Earth's late accretionary history" by König S. et al. [Earth Planet. Sci. Lett. 385 (2014) 110–121]. Earth Planet. Sci. Lett., 417: 167-169.

König, S., Schuth, S., Münker, C., Qopoto, C., 2007. The role of slab melting in the petrogenesis of high-Mg andesites: Evidence from Simbo Volcano, Solomon Islands, 153, 85-103 pp.

Kurzawa, T., Konig, S., Labidi, J., Yierpan, A., Schoenberg, R., 2017. A method for Se isotope analysis of low ng-level geological samples via double spike and hydride generation MC-ICP-MS. Chem. Geol., 466: 219-228.

Labidi, J., Cartigny, P., Moreira, M., 2013. Non-chondritic sulphur isotope composition of the terrestrial mantle. Nature, 501(7466): 208-211.

Labidi, J., Shahar, A., Le Losq, C., Hillgren, V.J., Mysen, B.O., Farquhar, J., 2016. Experimentally determined sulfur isotope fractionation between metal and silicate and implications for planetary differentiation. Geochim. Cosmochim. Acta, 175: 181-194.

Li, J.L., Gao, J., Klemd, R., John, T., Wang, X.S., 2016. Redox processes in subducting oceanic crust recorded by sulfide-bearing high-pressure rocks and veins (SW Tianshan, China). Contrib. Mineral. Petrol., 171:72(8-9).

Lissner, M., König, S., Luguet, A., le Roux, P., Schuth, S., Heuser, A., le Roex, A., 2014. Selenium and tellurium systematics in MORBs from the southern Mid-Atlantic Ridge (47–50 S). Geochim. Cosmochim. Acta, 144: 379-402.

Lorand, J.-P., Alard, O., 2010. Determination of selenium and tellurium concentrations in Pyrenean peridotites (Ariege, France): new insight into S/Se/Te systematics of the upper in mantle samples. Chem. Geol., 278(1): 120-130.

Luguet, A., Behrens, M., Pearson, D.G., König, S., Herwartz, D., 2015. Significance of the whole rock Re–Os ages in cryptically and modally metasomatised cratonic peridotites: Constraints from HSE–Se–Te systematics. Geochim. Cosmochim. Acta, 164: 441-463.

Mitchell, K., Mansoor, S.Z., Mason, P.R.D., Johnson, T.M., Van Cappellen, P., 2016. Geological evolution of the marine selenium cycle: Insights from the bulk shale δ82/76Se record and isotope mass balance modeling. Earth Planet. Sci. Lett., 441: 178-187.

Mottl, M.J., Wheat, C.G., Fryer, P., Gharib, J., Martin, J.B., 2004. Chemistry of springs across the Mariana forearc shows progressive devolatilization of the subducting plate. Geochim. Cosmochim. Acta, 68(23): 4915-4933.

Palme, H., O'Neill, H.S.C., 2014. 3.1 - Cosmochemical Estimates of Mantle Composition. In: Holland, H.D., Turekian, K.K. (Eds.), Treatise on Geochemistry (Second Edition). Elsevier, Oxford, pp. 1-39.

Park, J.-W., Campbell, I.H., Arculus, R.J., 2013. Platinum-alloy and sulfur saturation in an arc-related basalt to rhyolite suite: Evidence from the Pual Ridge lavas, the Eastern Manus Basin. Geochim. Cosmochim. Acta, 101: 76-95.

Pearce, J.A., Stern, R.J., Bloomer, S.H., Fryer, P., 2005. Geochemical mapping of the Mariana arc-basin system: Implications for the nature and distribution of subduction components. Geochemistry Geophysics Geosystems, 6.

Prytulak, J., Nielsen, S., Plank, T., Barker, M., Elliott, T., 2013. Assessing the utility of thallium and thallium isotopes for tracing subduction zone inputs to the Mariana arc. Chem. Geol., 345: 139-149.

Prytulak, J., Sossi, P.A., Halliday, A.N., Plank, T., Savage, P.S., Woodhead, J.D., 2017. Stable vanadium isotopes as a redox proxy in magmatic systems? Geochemical Perspectives Letters, 3(0): 75-84.

Rose-Weston, L., Brenan, J.M., Fei, Y., Secco, R.A., Frost, D.J., 2009. Effect of pressure, temperature, and oxygen fugacity on the metal-silicate partitioning of Te, Se, and S: Implications for earth differentiation. Geochim. Cosmochim. Acta, 73(15): 4598-4615.

Rouxel, O., Fouquet, Y., Ludden, J.N., 2004. Subsurface processes at the lucky strike hydrothermal field, Mid-Atlantic ridge: evidence from sulfur, selenium, and iron isotopes 1. Geochim. Cosmochim. Acta, 68(10): 2295-2311.

Rouxel, O., Ludden, J., Carignan, J., Marin, L., Fouquet, Y., 2002. Natural variations of Se isotopic composition determined by hydride generation multiple collector inductively coupled plasma mass spectrometry. Geochim. Cosmochim. Acta, 66(18): 3191-3199.

Schuth, S., König, S., Münker, C., 2011. Subduction zone dynamics in the SW Pacific plate boundary region constrained from high-precision Pb isotope data. Earth Planet. Sci. Lett., 311(3): 328-338.

Stern, R.J., Bloomer, S.H., 1992. Subduction Zone Infancy - Examples from the Eocene Izu-Bonin-Mariana and Jurassic California Arcs. Geol. Soc. Am. Bull., 104(12): 1621-1636.

Stern, R.J., Fouch, M.J., Klemperer, S.L., 2003. An overview of the Izu-Bonin-Mariana subduction factory. Inside the subduction factory, 138: 175-222.

Stern, R.J., Lin, P.-N., Morris, J.D., Jackson, M.C., Fryer, P., Bloomer, S.H., Ito, E., 1990. Enriched back-arc basin basalts from the northern Mariana Trough: implications for the magmatic evolution of back-arc basins. Earth Planet. Sci. Lett., 100(1): 210-225.

Stolper, E., Newman, S., 1994. The role of water in the petrogenesis of Mariana trough magmas. Earth Planet. Sci. Lett., 121(3): 293-325.

Stüeken, E.E., Buick, R., Bekker, A., Catling, D., Foriel, J., Guy, B.M., Kah, L.C., Machel, H.G., Montanez, I.P., Poulton, S.W., 2015. The evolution of the global selenium cycle: Secular trends in Se isotopes and abundances. Geochim. Cosmochim. Acta, 162: 109-125.

Tollstrup, D.L., Gill, J.B., 2005. Hafnium systematics of the Mariana arc: Evidence for sediment melt and residual phases. Geology, 33(9): 737-740.

Volpe, A.M., Douglas Macdougall, J., Lugmair, G.W., Hawkins, J.W., Lonsdale, P., 1990. Fine-scale isotopic variation in Mariana Trough basalts: evidence for heterogeneity and a recycled component in backarc basin mantle. Earth Planet. Sci. Lett., 100(1): 251-264.

Wang, Z., Becker, H., 2013. Ratios of S, Se and Te in the silicate Earth require a volatile-rich late veneer. Nature, 499(7458): 328-331.

Wang, Z., Becker, H., 2015. Comment on “A non-primitive origin of near-chondritic SSeTe ratios in mantle peridotites: Implications for the Earth's late accretionary history” by König S. et al. [Earth Planet. Sci. Lett. 385 (2014) 110–121]. Earth Planet. Sci. Lett., 417: 164-166.

Williams, H.M., Prytulak, J., Woodhead, J.D., Kelley, K.A., Brounce, M., Plank, T., 2018. Interplay of crystal fractionation, sulfide saturation and oxygen fugacity on the iron isotope composition of arc lavas: An example from the Marianas. Geochim. Cosmochim. Acta, 226: 224-243.

Yi, W., Halliday, A.N., Alt, J.C., Lee, D.C., Rehkamper, M., Garcia, M.O., Langmuir, C.H., Su, Y.J., 2000. Cadmium, indium, tin, tellurium, and sulfur in oceanic basalts: Implications for chalcophile element fractionation in the Earth. Journal of Geophysical Research-Solid Earth, 105(B8): 18927-18948.

Yierpan, A., König, S., Labidi, J., Kurzawa, T., Babechuk, M.G., Schoenberg, R., 2018. Chemical Sample Processing for Combined Selenium Isotope and Selenium-Tellurium Elemental Investigation of the Earth's Igneous Reservoirs. Geochem. Geophys. Geosyst., 19(2): 516-533.

Yierpan, A., König, S., Labidi, J., Schoenberg, R., 2019. Selenium isotope and S-Se-Te elemental systematics along the Pacific-Antarctic ridge: Role of mantle processes. Geochim. Cosmochim. Acta.

Fig. 1: Locality map for the Mariana arc system and locations of samples. Analyzed samples are from submarine seamounts (bold labels) and from two back-arc regions (shaded rectangular boxes). Modified after Alt et al. (1993 and references therein).

Fig. 2: Compilation of Se isotope compositions of Mariana lavas analyzed in this study and literature data. Data for deep-sea sediments, hydrothermal sulfides, hydrothermally altered basalts and the silicate Earth from Rouxel et al., (2002) are averaged values. Additional data for hydrothermal sulfides from Rouxel et al. (2004). Silicate Earth value by Rouxel et al. (2002) comprises a peridotite (PCC-1)

and five basalts (BHVO-1, BCR-1, BE-N and BR). 'basaltic lavas' (BHVO-2, BCR-2, BIR-1a, BE-N) from Yierpan et al. (2018). The vertical grey box indicates range of the Mariana pre-subduction mantle value that comprises basalts without any subduction-related origin measured by Yierpan et al. (2018) and the peridotite analyzed by Rouxel et al., (2002). PAR mantle represented by Pacific Antarctic Ridge MORBs (n=27) from Yierpan et al. (2019). Average values for Phanerozoic and Precambrian sediments from Stüeken et al. (2015). Range of global marine sediments from Mitchell et al., (2016) and references therein. All error bars given as 2 s.d. uncertainty, for details see section 3.3. No error bars displayed for hydrothermal sulfides as uncertainties exceed the diagram range (instead values are given).

Fig. 3: (a) Apparent covariation of collection depth and S concentrations, (b) no indication of eruption-related degassing of Se. (c) No covariation of collection depth and Se isotope composition, (d) S/Se vs. Se concentrations indicating S/Se not controlled by Se concentrations. All error bars given as 2 s.d..

Fig. 4: (a) Se, (b) Te and (c) Cu concentrations vs. MgO content show variation of chalcophile element concentrations as a function of their bulk partition coefficients during magmatic differentiation. (d) V/Sc ratio vs. MgO content, indicates V partitioning into magnetite and onset of the 'magnetite crisis' at ~3-4 wt.% MgO. Data for the Eastern Manus back-arc basin (EMBB) from Jenner et al., (2015 and references therein). PAR MORB data (light grey fields) from Yierpan et al. (2019). SMAR N-MORB (dark grey fields) data from Lissner et al. (2014). Copper concentration data of samples from the Central Island Province (CIP) of the Mariana system from Williams et al. (2018). Dashed vertical lines represent important stages during magmatic differentiation, see text for interpretation of the data.

Fig. 5: (a) Se isotope compositions of Mariana lavas vs. MgO contents shows no covariation with index of alteration indicating absence of isotope fractionation during magmatic differentiation. (b) Se isotope composition of Mariana lavas vs. Se concentrations indicates no isotope fractionation during magmatic differentiation (i.e. sulfide segregation, alloy fractionation; see text for details).

Fig. 6: (a) Ba/Th vs. Th/Yb indicating different proportions of slab-derived components. Se isotope composition vs. (b) Ba/Th and (c) Th/Yb indicating the influence of slab-derived fluid and melt-like components. (d) Se isotope composition vs. Ba/Yb demonstrates Se isotope composition as function of total subduction addition. See section 5.3 for details. Labelled boxes in (b) point to Se isotope compositions of deep-sea sediments (ODP 1149 Leg 185), hydrothermally altered basalt and hydrothermal sulfides analyzed by Rouxel et al., (2002, 2004). White box indicates Mariana pre-subduction mantle wedge value (0.23±0.12‰, 2 s.d., n=5) represented by non-subduction-related mantle melts (basalts, Yierpan et al., 2018; peridotite, Rouxel et al., 2002) and. Ba/Th, Th/Yb and Ba/Yb ratios for the (sub-arc) mantle taken from Gale et al. (2013). All error bars given as 2 s.d..

Fig. A.1: Extended multi-element diagram for Mariana samples . Element order modified after Williams et al. (2018) and element concentrations normalized to primitive mantle estimates from Palme and O'Neill (2014 and references therein).

Fig. A.2: (a) Se isotope composition vs. La/Sm ratio shows evidence for melt-like component in the Mariana arc samples similar to what is inferred from Figure 6 c and d; Se isotope composition vs. Th/Yb and Ba/Yb, respectively.

Table 1: Combined Se isotope compositions and Se-Te concentrations of Mariana samples and international rock reference materials (United States Geological Survey, USGS; Geological Survey of Japan, GSJ).

Table 1 Footnote: Se isotope data reported relative to Se reference solution NIST SRM-3149. *Samples 1881-4 and 1880-3 (K2) were used to assess external reproducibility, see table A.1. ┼Uncertainty on Se isotope compositions is conservatively set to be 0.10 ‰ as derived from multiple digested and analyzed samples during different measurement sessions. **BHVO-2 was analyzed together with Mariana samples and published by Yierpan et al. (2018) with long-term BHVO-2 reproducibility of 0.18±0.10‰ (2 s.d., n=8, multiple analytical sessions over 6 months). Uncertainty on Se-Te concentrations conservatively expressed as 3% relative standard deviation. $^{\pi}$S concentrations from Alt et al. (1993). For reference concentration data of GSJ JB-2 and JB-3 see Table A.1.

Figure 1

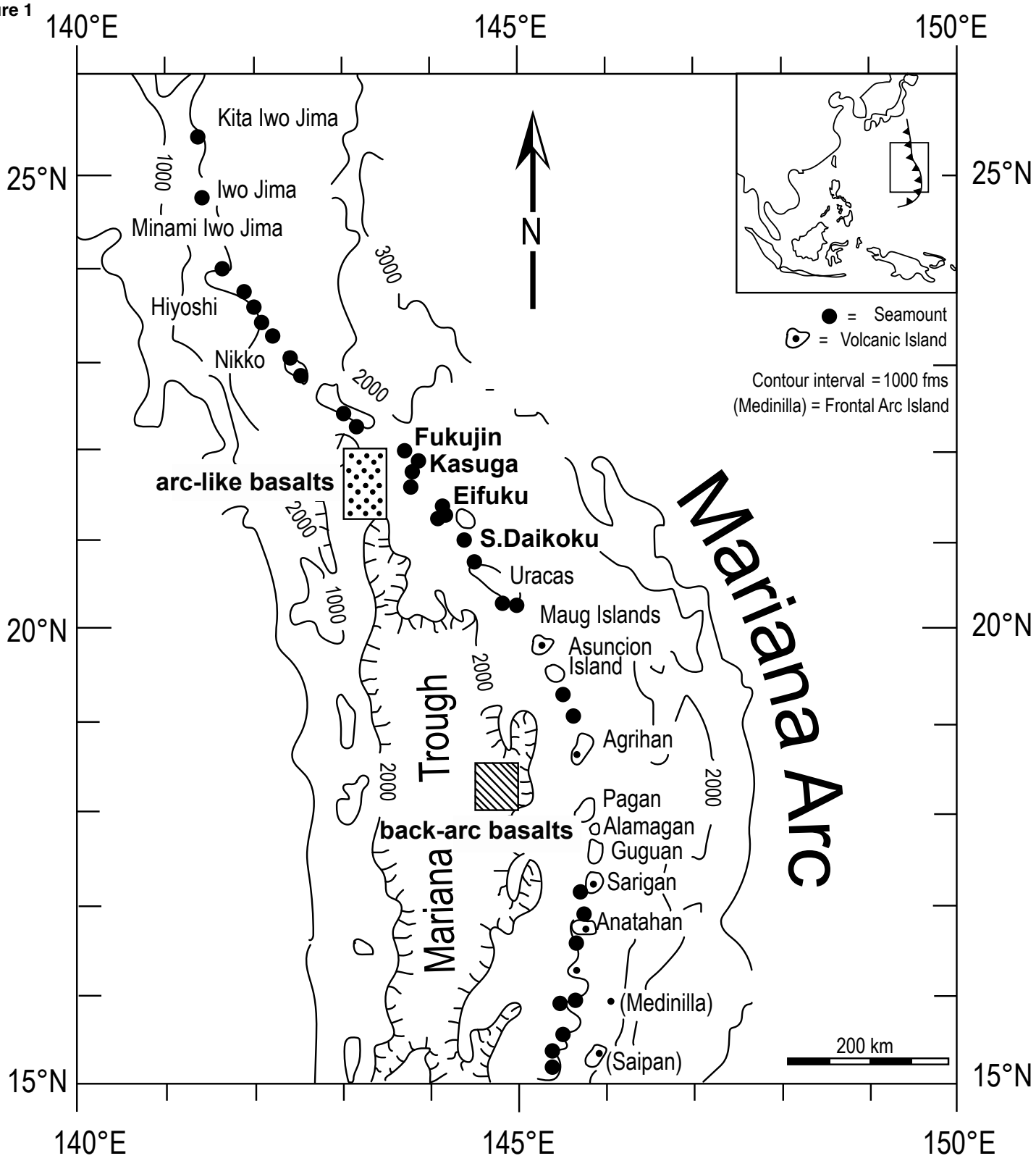
140°E
145°E
150°E
25°N
20°N
15°N
Kita Iwo Jima
Iwo Jima
Minami Iwo Jima
Hiyoshi
Nikko
1000
2000
3000
N
= Seamount
= Volcanic Island
Contour interval = 1000 fms
(Medinilla) = Frontal Arc Island
Fukujin
Kasuga
Eifuku
S.Daikoku
Uracas
Maug Islands
Asuncion Island
Agrihan
Pagan
Alamagan
Guguan
Sarigan
Anatahan
(Medinilla)
(Saipan)
arc-like basalts
back-arc basalts
Trough
Mariana
Mariana Arc
200 km

Figure 2

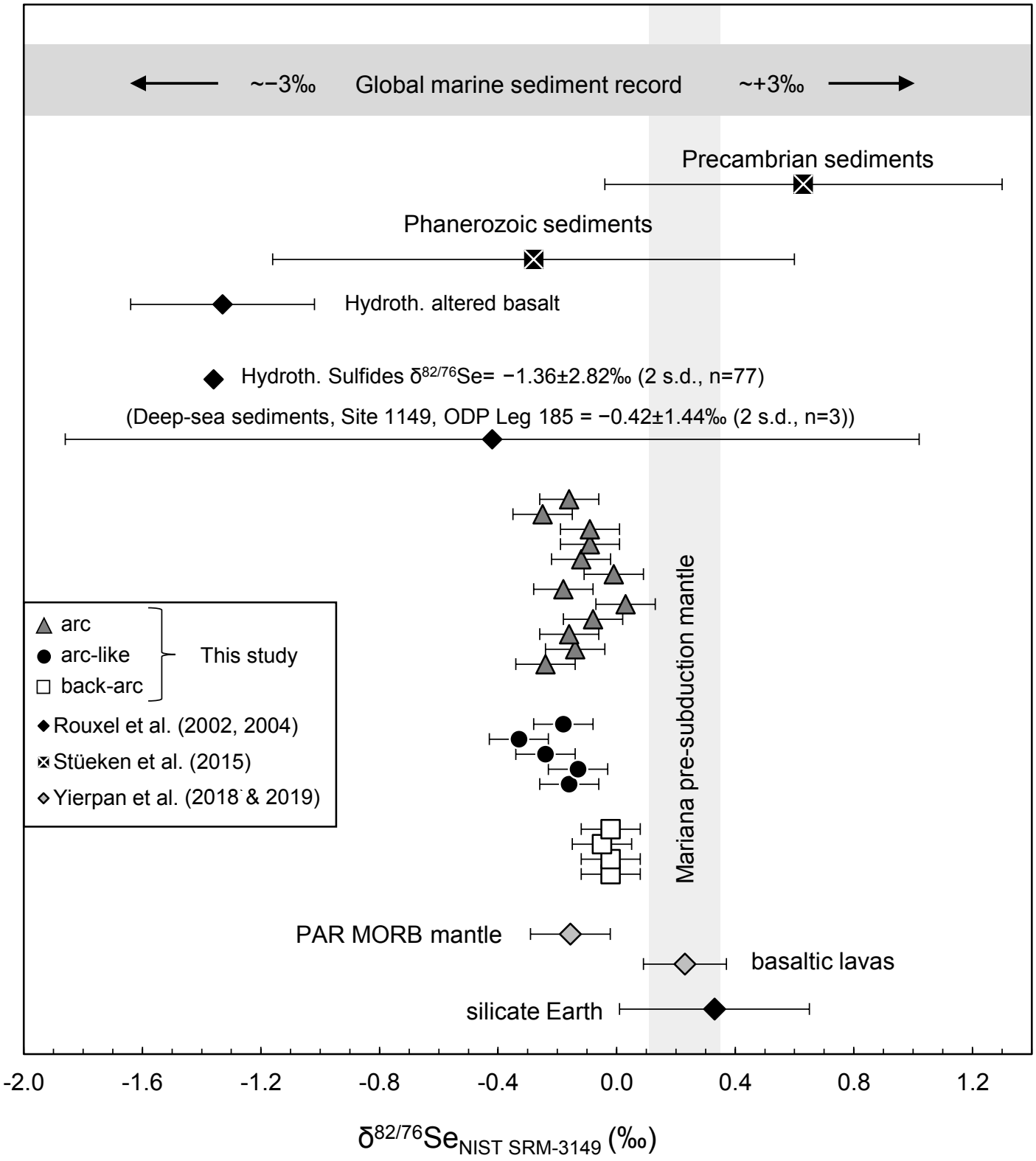
~−3‰
Global marine sediment record
~+3‰
Precambrian sediments
Phanerozoic sediments
Hydroth. altered basalt
Hydroth. Sulfides δ82/76Se= −1.36±2.82‰ (2 s.d., n=77)
(Deep-sea sediments, Site 1149, ODP Leg 185 = −0.42±1.44‰ (2 s.d., n=3))
arc
arc-like
back-arc
This study
Rouxel et al. (2002, 2004)
Stüeken et al. (2015)
Yierpan et al. (2018 & 2019)
Mariana pre-subduction mantle
PAR MORB mantle
basaltic lavas
silicate Earth
-2.0
-1.6
-1.2
-0.8
-0.4
0.0
0.4
0.8
1.2
δ82/76SeNIST SRM-3149 (‰)

Figure 3

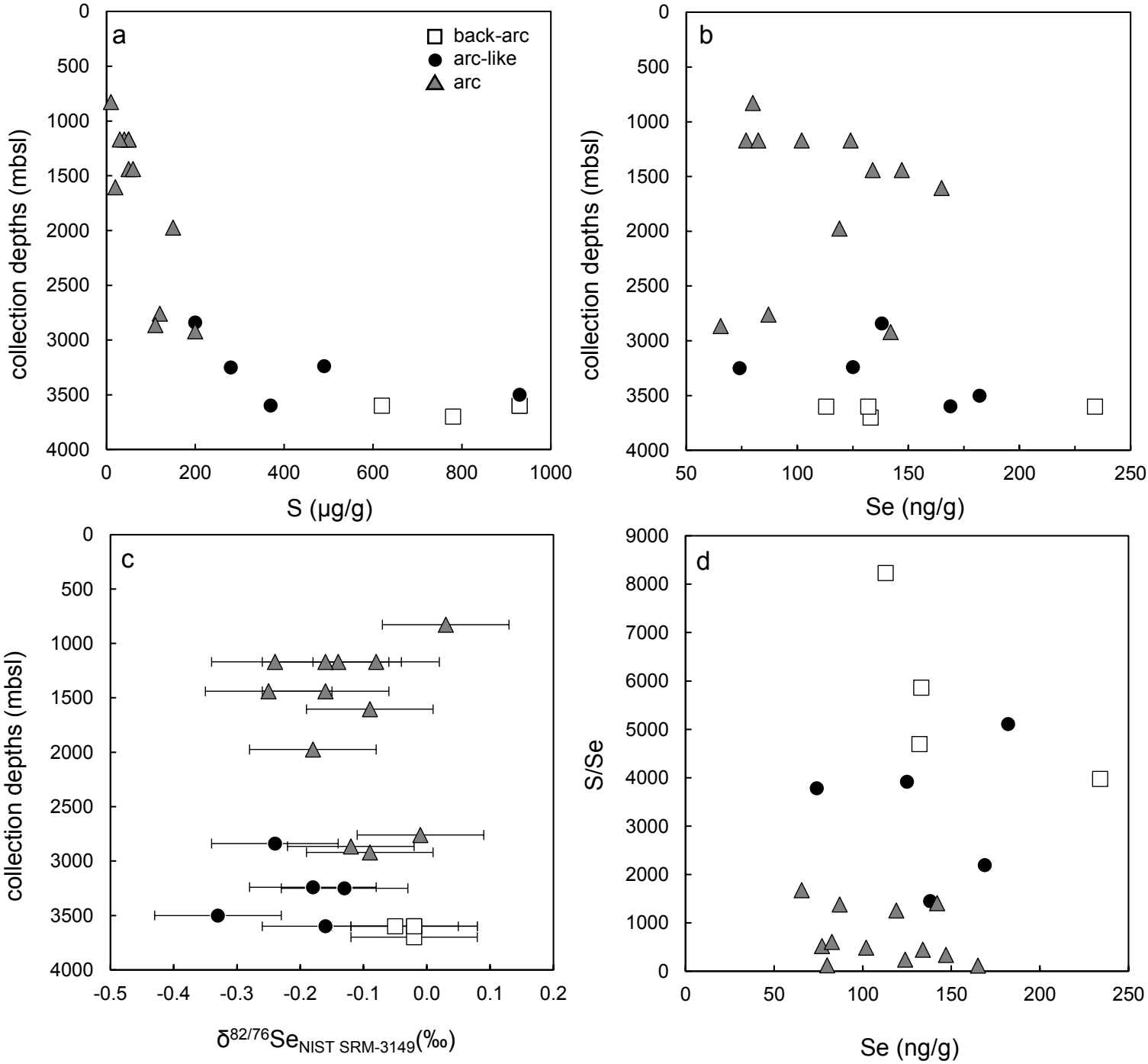
a
back-arc
arc-like
arc
collection depths (mbsl)
S (μg/g)
b
Se (ng/g)
c
δ82/76SeNIST SRM-3149(‰)
d
S/Se

Figure 4

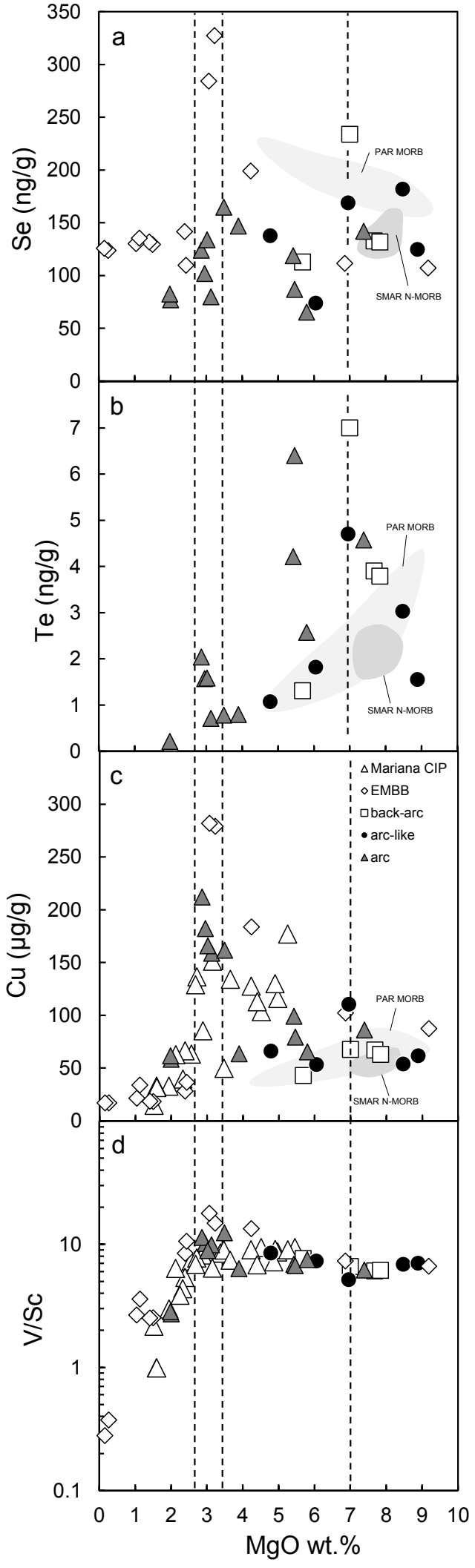
a
b
c
d
Se (ng/g)
Te (ng/g)
Cu (µg/g)
V/Sc
MgO wt.%
PAR MORB
SMAR N-MORB
Mariana CIP
EMBB
back-arc
arc-like
arc

Figure 5

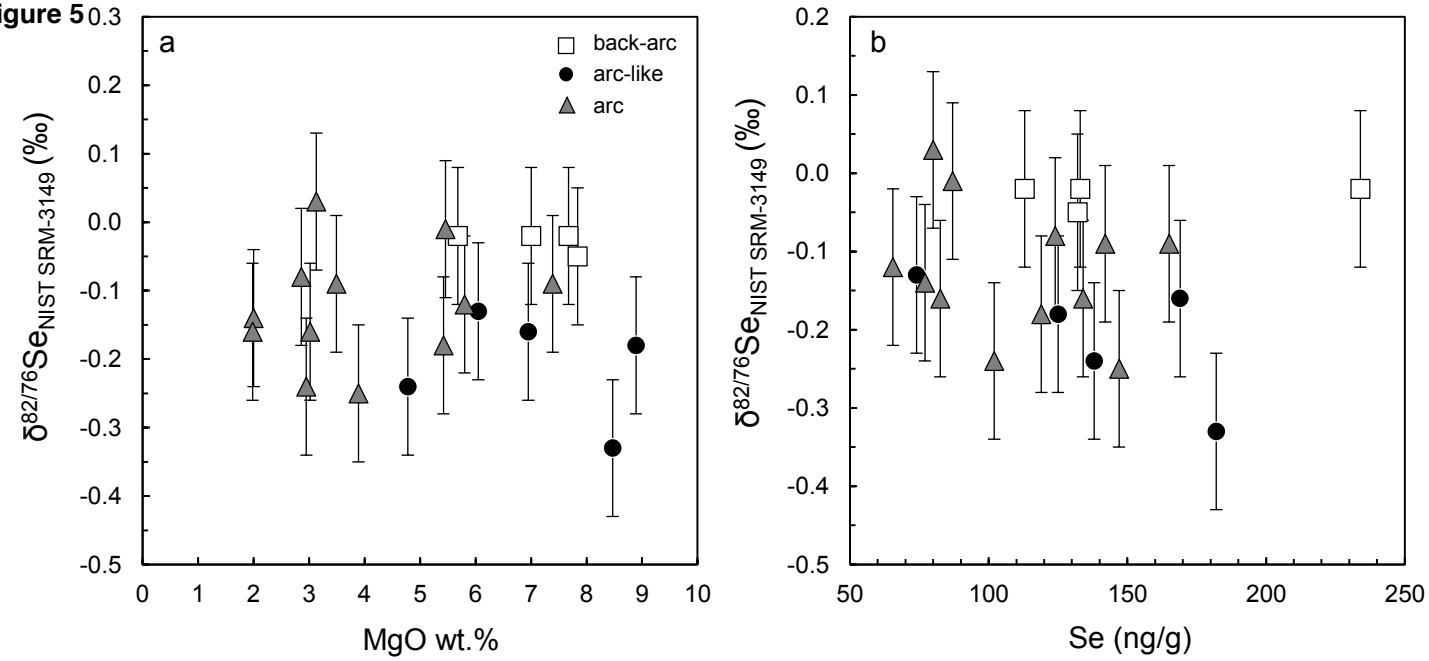
a
back-arc
arc-like
arc
δ82/76SeNIST SRM-3149 (‰)
MgO wt.%
b
δ82/76SeNIST SRM-3149 (‰)
Se (ng/g)

Figure 6

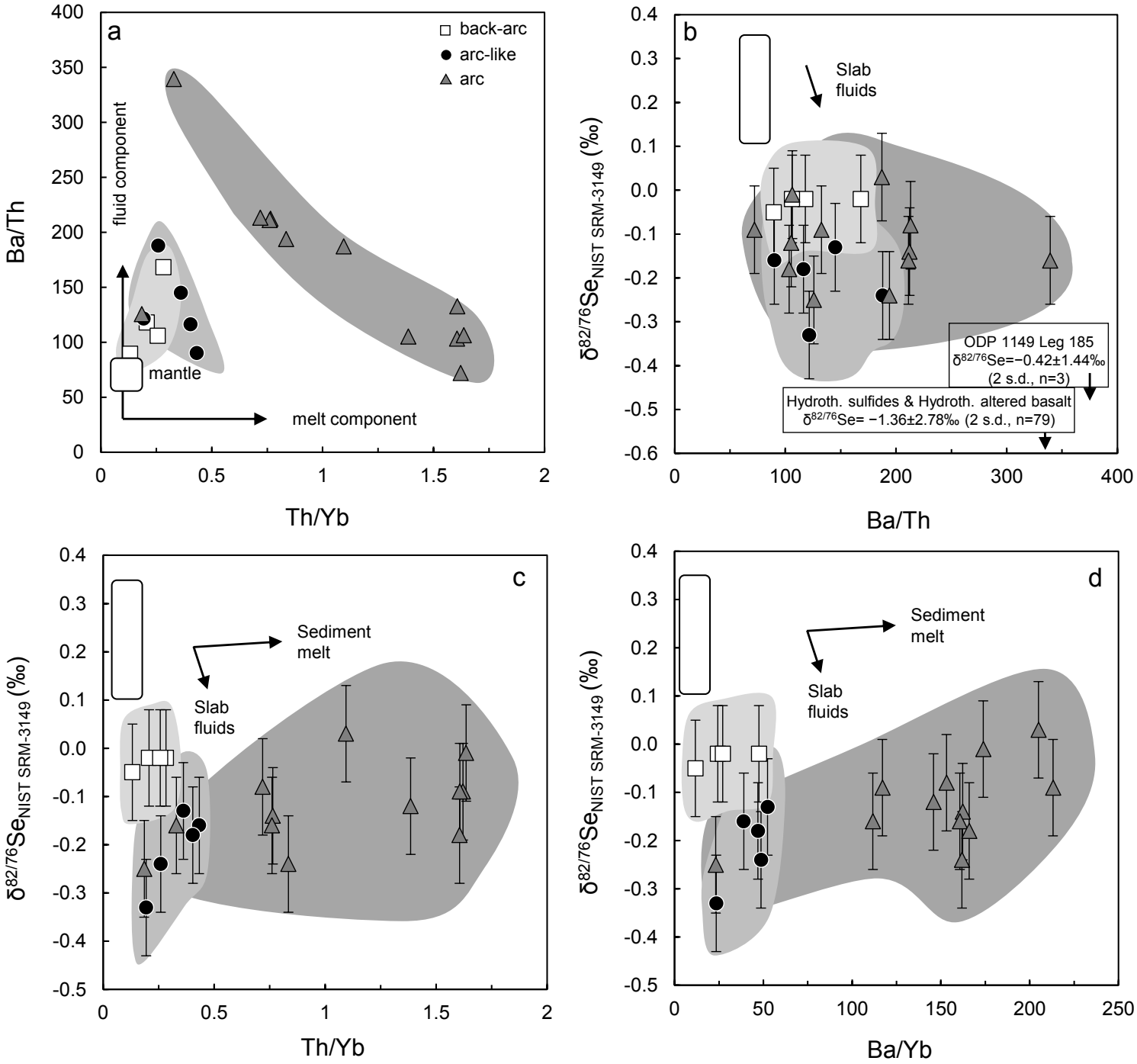
a
back-arc
arc-like
arc
fluid component
mantle
melt component
Ba/Th
Th/Yb
b
Slab
fluids
ODP 1149 Leg 185
δ82/76Se=−0.42±1.44‰
(2 s.d., n=3)
Hydroth. sulfides & Hydroth. altered basalt
δ82/76Se= −1.36±2.78‰ (2 s.d., n=79)
δ82/76SeNIST SRM-3149 (‰)
Ba/Th
c
Sediment
melt
Slab
fluids
δ82/76SeNIST SRM-3149 (‰)
Th/Yb
d
Sediment
melt
Slab
fluids
δ82/76SeNIST SRM-3149 (‰)
Ba/Yb

Tab. 1: Combined Se isotope compositions and Se−Te concentrations of Mariana samples and international rock reference materials (United States Geological Survey, USGS; Geological Survey of Japan, GSJ).

sample	location	Rock type	SiO_2 wt.%	MgO wt.%	analyses n	$\delta^{82/76}$Se (‰)	2 s.d.† (‰)	Se (ng/g)	1 s.d. (ng/g)	Te (ng/g)	1 s.d. (ng/g)	Se/Te	S (µg/g)
15161	arc, Fukujin	andesite	58.0	2.95	1	−0.24	0.10	102	3	1.57	0.05	65	50
1580	arc, Fukujin	andesite	59.7	2.00	1	−0.14	0.10	77	2	0.16	<0.01	481	40
15117	arc, Fukujin	andesite	60.6	1.98	1	−0.16	0.10	83	2	0.21	<0.01	393	50
15146	arc, Fukujin	andesite	56.7	2.86	1	−0.08	0.10	124	4	2.04	0.06	61	30
D35−1−4	arc, Fukujin	andesite	56.0	3.13	2	0.03	0.10	81	2	0.71	0.02	113	10
1880−3 (K2)*	arc, Kasuga	basalt	51.2	5.42	6	−0.18	0.10	119	4	4.21	0.13	28	150
1883−5 (P)	arc, Kasuga	bas. andesite	52.3	5.46	1	−0.01	0.10	87	3	6.40	0.19	14	120
1885−6 (K3)	arc, Kasuga	bas. andesite	54.6	5.80	2	−0.13	0.10	66	2	2.57	0.08	25	110
1884−10 (K3)	arc, Kasuga	absarokite	50.3	7.39	2	−0.09	0.10	142	4	4.57	0.14	31	200
D31−3−1	arc, Eifuku	bas. andesite	52.7	3.49	1	−0.09	0.10	165	5	0.78	0.02	212	20
D25−3	arc, S.Daikoku	bas. andesite	54.2	3.89	1	−0.25	0.10	147	4	0.79	0.02	186	50
D25−1−4	arc, S.Daikoku	andesite	57.5	3.02	1	−0.16	0.10	134	4	1.58	0.05	85	60
1838−13	back−arc, 18°N	bas. andesite	52.7	5.68	2	−0.03	0.10	113	3	1.31	0.04	86	930
1839−3	back−arc, 18°N	basalt	48.5	7.68	1	−0.02	0.10	133	4	3.90	0.12	34	780
1841−18	back−arc, 18°N	basalt	50.5	7.84	1	−0.05	0.10	132	4	3.79	0.11	35	620
1846−12	back−arc, 18°N	basalt	50.8	7.00	2	−0.02	0.10	234	7	7.00	0.21	33	930
1846−9	arc−like, 18°N	basalt	49.7	6.95	1	−0.16	0.10	169	5	4.70	0.14	36	370
1881−4*	arc−like, 22°N	bas. andesite	53.0	6.05	3	−0.13	0.10	74	2	1.82	0.05	41	280
D65−4	arc−like, 22°N	bas. andesite	53.9	4.78	2	−0.25	0.10	138	4	1.07	0.03	129	200
D67−10	arc−like, 22°N	basalt	49.8	8.47	1	−0.33	0.10	182	5	3.03	0.09	60	930
D68−4	arc−like, 22°N	basalt	50.4	8.89	1	−0.18	0.10	125	4	1.55	0.05	81	490
USGS BHVO−2**		basalt			1	0.16	0.10	166	5	14.1	0.42	12	
GSJ JB−2		basalt			3	−0.19	0.10	153	5	3.78	0.11	40	
GSJ JB−3		basalt			2	0.16	0.10	67	2	1.03	0.03	65	

Se isotope data reported relative to Se reference solution NIST SRM-3149. *Samples 1881-4 and 1880-3 (K2) were used to assess external reproducibility, see table A.1. †Uncertainty on Se isotope compositions is conservatively set to be 0.10 ‰ as derived from multiple digested and analyzed samples during different measurement sessions. ** BHVO-2 was analyzed together with Mariana samples and published by Yierpan et al. (2018) as part of a study assessing long-term BHVO-2 reproducibility, which is $\delta^{82/76}$Se=0.18±0.10‰ (2 s.d., n=8, multiple analytical sessions over 6 months). Uncertainty on Se-Te concentrations conservatively expressed as 3% relative standard deviation. For reference concentration data of GSJ JB-2 and JB-3 see table A.1.

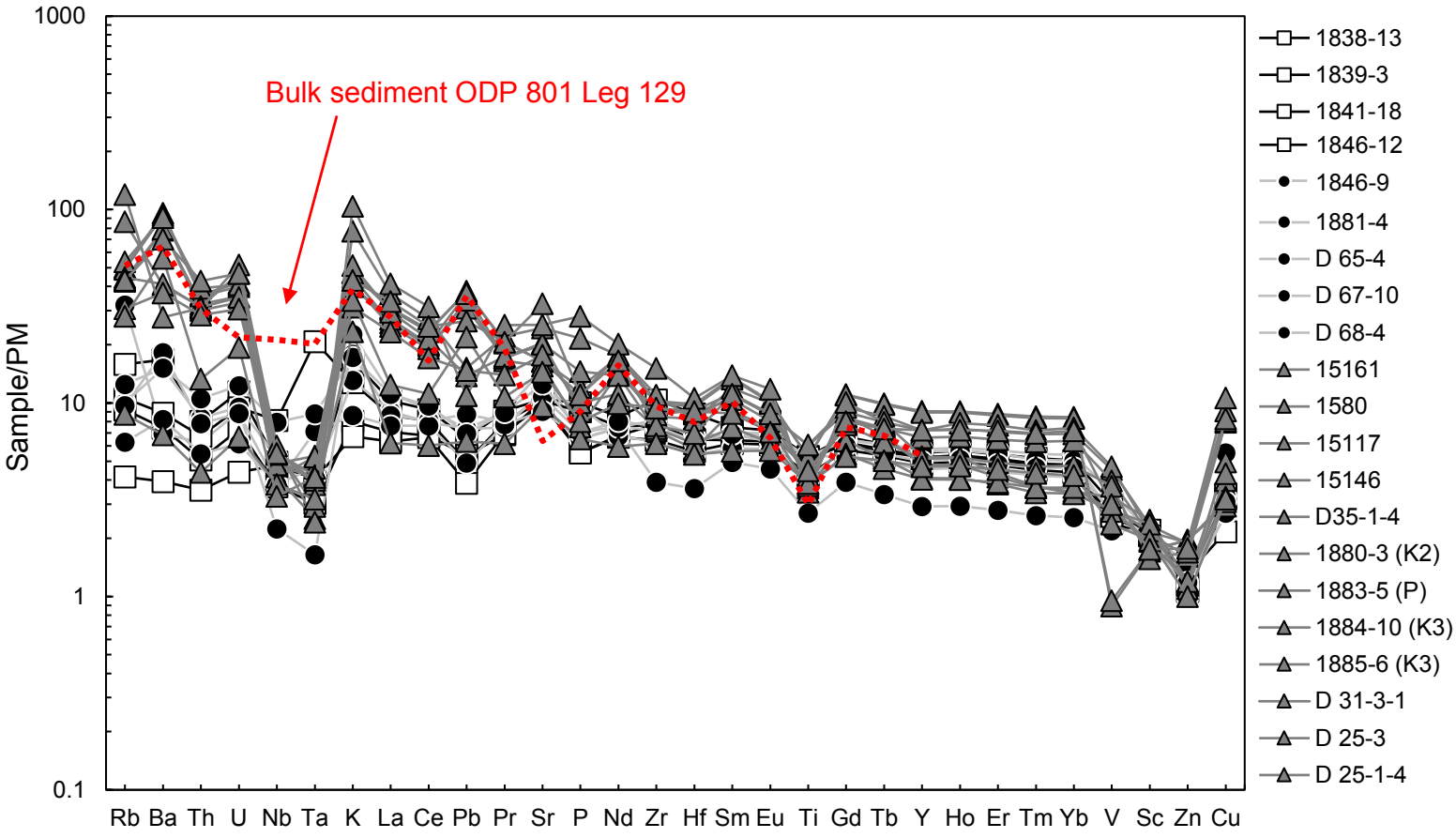
Bulk sediment ODP 801 Leg 129
Sample/PM
1000
100
10
1
0.1
Rb Ba Th U Nb Ta K La Ce Pb Pr Sr P Nd Zr Hf Sm Eu Ti Gd Tb Y Ho Er Tm Yb V Sc Zn Cu
1838-13
1839-3
1841-18
1846-12
1846-9
1881-4
D 65-4
D 67-10
D 68-4
15161
1580
15117
15146
D35-1-4
1880-3 (K2)
1883-5 (P)
1884-10 (K3)
1885-6 (K3)
D 31-3-1
D 25-3
D 25-1-4

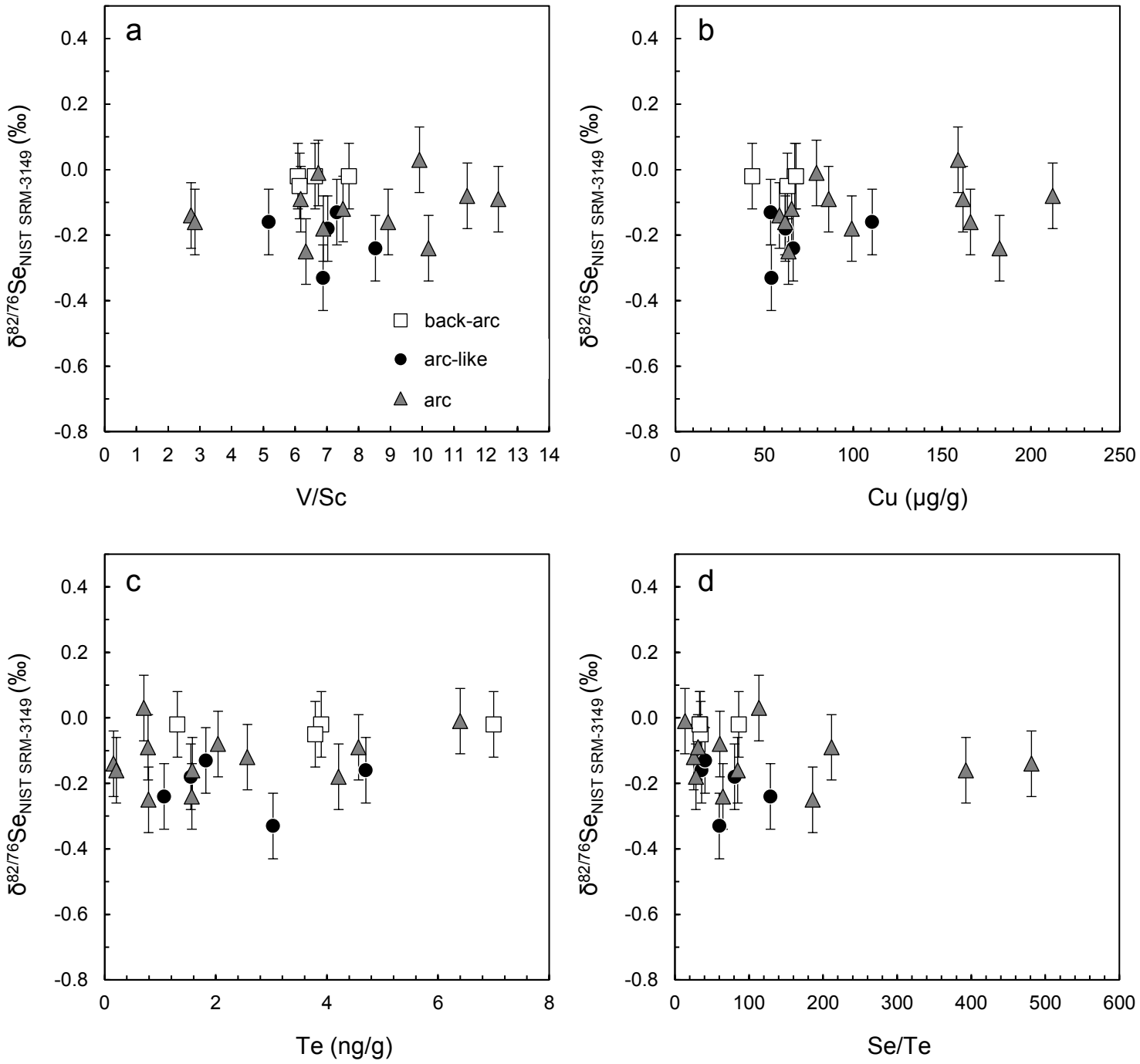
a
b
c
d
back-arc
arc-like
arc
δ82/76SeNIST SRM-3149 (‰)
V/Sc
Cu (μg/g)
Te (ng/g)
Se/Te

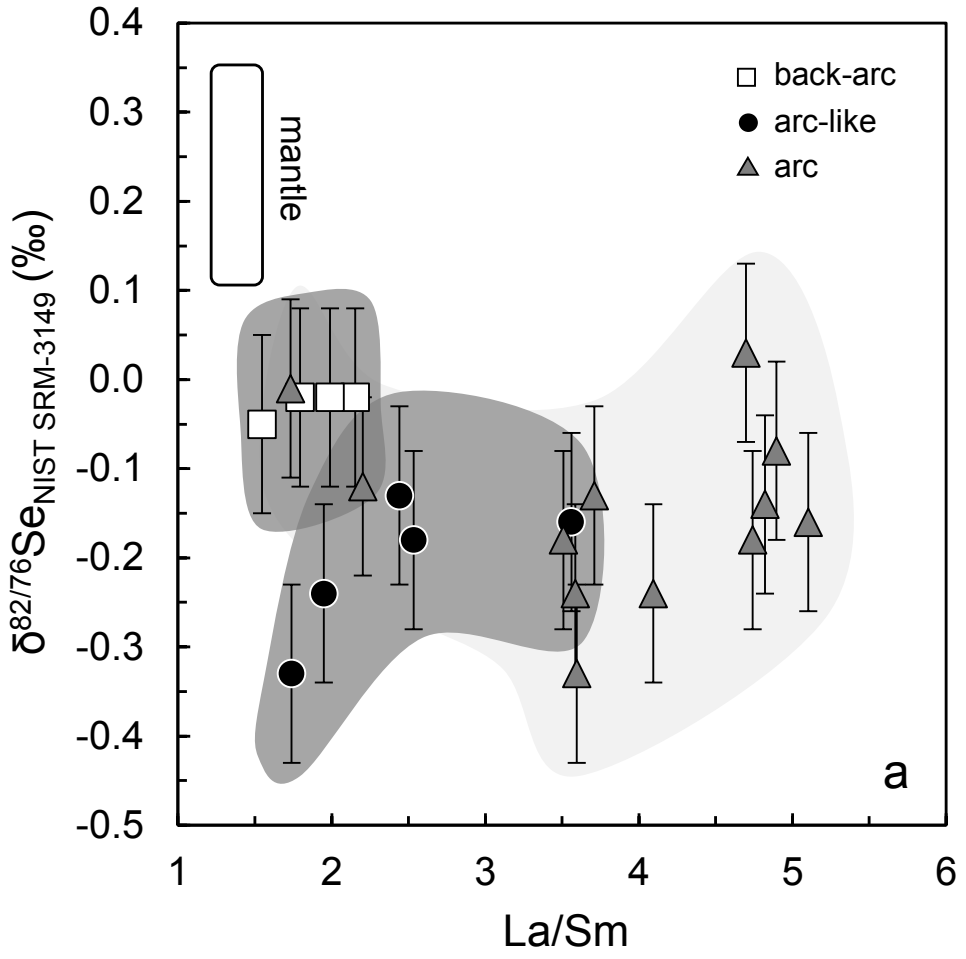
back-arc
arc-like
arc
mantle
a
δ82/76SeNIST SRM-3149 (‰)
La/Sm

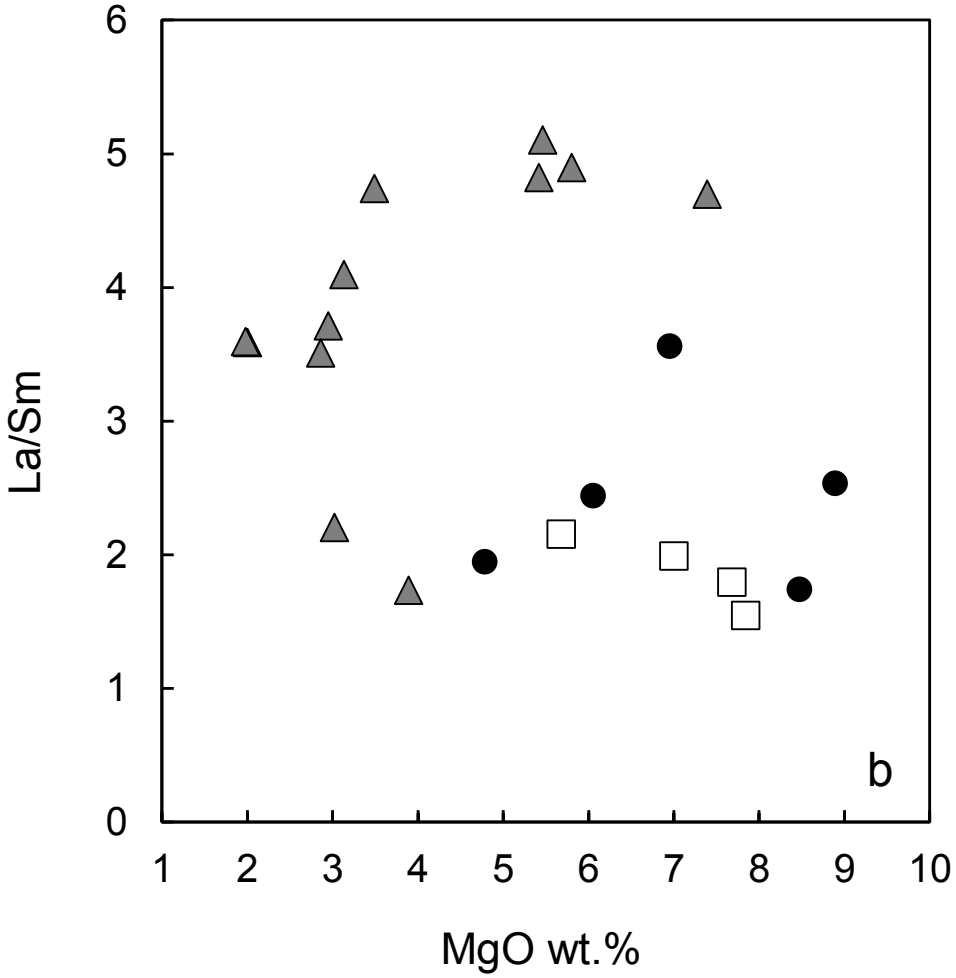
b
La/Sm
MgO wt.%